



PAPER

OPEN ACCESS

RECEIVED

18 September 2023

REVISED

20 February 2024

ACCEPTED FOR PUBLICATION

29 February 2024

PUBLISHED

13 March 2024

Original Content from this work may be used under the terms of the [Creative Commons Attribution 4.0 licence](https://creativecommons.org/licenses/by/4.0/).

Any further distribution of this work must maintain attribution to the author(s) and the title of the work, journal citation and DOI.



Nonuniformly twisted states and traveling chimeras in a system of nonlocally coupled identical phase oscillators

L A Smirnov¹ , M I Bolotov^{1,*} and A Pikovsky²

¹ Department of Control Theory, Research and Education Mathematical Center ‘Mathematics for Future Technologies’, Nizhny Novgorod State University, Gagarin Av. 23, 603022 Nizhny Novgorod, Russia

² Department of Physics and Astronomy, University of Potsdam, Karl-Liebknecht-Str. 24/25, 14476 Potsdam-Golm, Germany

* Author to whom any correspondence should be addressed.

E-mail: maxim.i.bolotov@gmail.com

Keywords: twisted states, traveling chimera, phase oscillators, Lyapunov exponent, nonlocal coupling, asymmetric coupling

Abstract

We explore the model of a population of nonlocally coupled identical phase oscillators on a ring (Abrams and Strogatz 2004 *Phys. Rev. Lett.* **93** 174102) and describe traveling patterns. In the continuous in space formulation, we find families of traveling wave solutions for left-right symmetric and asymmetric couplings. Only the simplest of these waves are stable, which is confirmed by numerical simulations for a finite population. We demonstrate that for asymmetric coupling, a weakly turbulent traveling chimera regime is established, both from an initial standing chimera or an unstable traveling wave profile. The weakly turbulent chimera is a macroscopically chaotic state, with a well-defined synchronous domain and partial coherence in the disordered domain. We characterize it through the correlation function and the Lyapunov spectrum.

1. Introduction

The collective dynamics of oscillator ensembles attracts much interest across different fields of science and engineering. One of the paradigmatic and universal objects of study is the model of nonlocally coupled phase oscillators. The theoretical and experimental investigations have shown that such systems possess so-called chimera states [1]. These symmetry-broken states are characterized by the coexistence of synchronous and asynchronous groups of oscillators [1–3]. Kuramoto and Battogtokh (KB) [4] observed and explained the first chimera regime for a ring of interacting phase oscillators with an exponential kernel. Then, Abrams and Strogatz (AS) [5] proposed an alternative version of the convolution operator kernel, represented as a combination of zero and first Fourier modes. This assumption allowed them to describe chimeras semi-analytically using the Ott–Antonsen (OA) approach [6–8]. Note, in the works [9–12], it has been shown that for the KB model, many theoretical results can be obtained by modifying the exponential kernel by accounting for periodic boundary conditions. Chimera regimes, discovered by Kuramoto and Battogtokh almost 20 years ago, continue to be in the focus of theoretical and experimental studies [1–3].

While chimeras are typically standing synchronization patterns, the possibility of localized traveling synchronization waves in oscillatory media has also been explored and demonstrated. Recently, Omel’chenko [13, 14] has studied the AS model with asymmetry in the interaction of nonidentical phase oscillators (with heterogeneous natural frequencies) and observed nontrivial patterns in the form of traveling waves moving at constant velocities. These traveling waves have been expressed in terms of the coarse-grained order parameter within the OA approach, but the limiting case of identical oscillators was not treated. Hence, the possibility of such traveling waves in purely regular oscillatory media remains an open problem. Our work is aimed at bridging this gap.

Traveling waves on a ring can appear as so-called twisted states [15–19]. In a uniformly twisted state, the phase difference between adjacent oscillators is a constant, such that the total phase shift around the ring is an integer multiple of 2π . This type of collective modes, which, because of a linear in space profile of the phases is sometimes called plane wave solution, is an important yet simple coherent regime of oscillator population dynamics. In the recent paper [20], nonuniformly twisted states with nonuniform phase profiles

were reported in a ring of nonlocally symmetrically coupled Stuart–Landau oscillators. They are characterized by a nonconstant gradient of the ordered phase distribution and an inhomogeneous amplitude profile that travels along the ring with a fixed shape and a constant speed. However, in the present work, we show that the spatiotemporal amplitude variations are not necessarily needed to form such collective modes and they can exist in the phase-reduced model (e.g. in the AS setup).

We mention here other known examples of traveling solutions. In [18], two types of traveling patterns (regular phase profiles and chimera-like states) in a system of identical units with symmetric in space coupling have been reported. Synchronization waves (moving patterns of different degrees of local synchrony) have been reported in systems with local coupling [21] and with a combination of global and local coupling [22]. In paper [23], the authors considered a ring of identical oscillators with an asymmetric KB-type coupling. They observed a chimera-like state, although they followed this motion for a relatively short time interval. This system is close to the KB setup, with an additional advective term in the coupling [24]. The basic observation is that a relatively ordered phase profile appears in such a system, which, however, can be well visualized for a large number of oscillators only. This traveling regime is non-stationary and weakly turbulent. Additionally, in [24], regular traveling wave solutions in a KB-type setting were constructed, but only some of them are stable.

The present paper is based on the AS setup, with an additional asymmetric term in the coupling. Typical patterns observed in such a spatially extended system closed in a ring are nonuniformly twisted states and traveling turbulent (irregularly changing) wave patterns resembling chimera states. Combining numerical simulations with analytical consideration, we conduct a detailed study of these regimes. We describe and characterize them both qualitatively and quantitatively, determining their most important properties. The reported observations in the AS setup significantly extend the previous findings by clarifying what happens for identical oscillators in the case of asymmetric coupling.

2. Basic model

2.1. Continuous and discrete setups

Our basic model is a generalization of the setup [5] for a population of nonlocally coupled phase oscillators arranged in a ring. In a continuous formulation, at each position on the ring $0 \leq x < 2\pi$, a phase $\varphi(x, t)$ is defined, which is governed by a local driving complex field $H(x, t)$:

$$\frac{\partial \varphi(x, t)}{\partial t} = \text{Im} \left(H(x, t) e^{-i\varphi(x, t) - i\alpha} \right). \quad (1)$$

Without loss of generality, we assumed that the natural frequencies of the oscillators are the same and set this frequency to zero by choosing the appropriate rotating reference frame. The phase shift α is the essential parameter of the model. The driving field $H(x, t)$ is a weighted sum of contributions from all the oscillators with a kernel $G(x)$:

$$H(x, t) = \int_{-\pi}^{\pi} G(x - \zeta) e^{i\varphi(\zeta, t)} d\zeta. \quad (2)$$

In the presented work, the function $G(x)$ is chosen in the following specific form:

$$G(x) = (g_0 + g_1 \cos x + g_2 \sin x) / 2\pi. \quad (3)$$

In the original AS model, the kernel $G(x)$ is supposed to be symmetric, i.e. $g_2 = 0$, while, in this work, we also account for a possible asymmetry $\sim g_2$ in the nonlocal coupling of the particle, following [13, 14, 25].

According to [13, 14, 25], such an asymmetry can lead to several interesting effects on the collective behavior of oscillators. By rescaling time, we can set $g_0 = 1$, which will be assumed throughout the paper. Thus, the governing parameters are α , g_1 and g_2 .

In direct numerical simulations, we use a discretization of the continuous setup (1), (2), by considering N equidistributed oscillators on the circle. The resulting system of ordinary differential equations (ODEs) reads

$$\frac{d\varphi_n}{dt} = \text{Im} \left(H_n(t) e^{-i\varphi_n(t) - i\alpha} \right), \quad (4)$$

where each unit is subject to a driving force from the complex mean field

$$H_n(t) = \sum_{\tilde{n}=1}^N G_{n, \tilde{n}} e^{i\varphi_{\tilde{n}}(t)}, \quad (5)$$

and the coupling coefficients $G_{n,\tilde{n}}$ are defined by relations

$$G_{n,\tilde{n}} = 2\pi G(2\pi(n - \tilde{n})/N)/N. \quad (6)$$

2.2. Coarse-grained complex order parameter

In general, $\varphi(x, t)$ is a measurable, non-continuous function of space. To characterize the distribution of the phases, it is convenient to introduce a coarse-grained (local) order parameter

$$Z(x, t) = \left\langle e^{i\varphi(\zeta, t)} \right\rangle_{\zeta \in (x-\delta, x+\delta)} = \frac{1}{2\delta} \int_{x-\delta}^{x+\delta} e^{i\varphi(\zeta, t)} d\zeta, \quad (7)$$

where the last integral is understood in the Lebesgue sense. The interval δ should be much smaller than all other characteristic spatial scales. If the local distribution of the phases is a delta-distribution (local synchrony), then $Z(x, t) = e^{i\bar{\varphi}(x, t)}$, where $\bar{\varphi}(x, t)$ is a continuous in space local phase. If the local distribution of the phases is uniform, then $Z(x, t) = 0$. In general, the $|Z(x, t)|$ value characterizes the local synchrony level.

3. Traveling wave solutions

In this section, we describe particular continuous in space solutions. Because of the ring geometry, such solutions are characterized by a topological integer parameter M (winding number), which is defined according to

$$M = \frac{\varphi(x + 2\pi, t) - \varphi(x, t)}{2\pi}. \quad (8)$$

We will seek for traveling waves

$$\varphi(x, t) = \phi(\xi) + \Omega t, \quad H(x, t) = h(\xi) e^{i\Omega t}, \quad (9)$$

with the traveling coordinate $\xi = x - vt$. Parameters Ω and v determine the wave's frequency and velocity. The winding number enters as a periodicity condition

$$\phi(\xi) = \phi(\xi + 2\pi) - 2\pi M. \quad (10)$$

3.1. Uniformly twisted states

The simplest traveling waves have a linear in space profile. The solution satisfying the boundary condition (10) has a form

$$\varphi(x, t) = \phi_0 + Mx + \Omega_M t, \quad (11)$$

where ϕ_0 is an arbitrary constant. A substitution in the basic equations yields the following expression for the frequency Ω_M :

$$\Omega_M = \begin{cases} -\sin \alpha & \text{if } M = 0, \\ -(g_1 \sin \alpha + Mg_2 \cos \alpha)/2 & \text{if } |M| = 1, \\ 0 & \text{if } |M| > 2. \end{cases} \quad (12)$$

Notably, the case $M=0$ corresponds to a fully synchronous state with a constant in space phase.

The stability properties of these solutions, characterized by parameters Ω_M and M , can be analytically studied using a standard linearization procedure near the respective mode. In this way, we arrive at the eigenvalue problem, analyzing which, we obtain the following results:

- (a) the homogeneous synchronous state with $M=0$ is stable if $\cos \alpha > 0$ and $0 < g_1 < 2$;
- (b) the stability condition of uniformly twisted modes with $M = \pm 1$ consists in the simultaneous fulfillment of three inequalities $g_1 \cos \alpha + Mg_2 \sin \alpha > 0$, $g_1 \cos \alpha + 3Mg_2 \sin \alpha > 0$, and $(g_1 - 1) \cos \alpha + Mg_2 \sin \alpha > 0$;
- (c) the uniformly twisted states with $|M| > 1$ is stable if $\cos \alpha < 0$ and $g_1 > 0$.

Here, in addition, we emphasize that the homogeneous fully asynchronous regime is stable if $\cos \alpha < 0$ and $g_1 > |g_2 \tan \alpha|$. Technical details of such a stability analysis can be found in [15, 18]. Note that one can perform this analysis employing relations presented below for a more general inhomogeneous in space situation.

Finally, we stress that the uniformly twisted states with spatial rotation number $|M| > 1$ correspond to vanishing velocity v in (9). In contradistinction, the uniformly twisted states with the spatial rotation number $M = \pm 1$ can be represented in the form of genuine traveling waves because the frequency Ω_M differs from zero in this case: $\varphi(x, t) = \pm \xi = \pm(x - vt)$ where $v = -\Omega_{\pm 1} = (g_1 \sin \alpha \pm g_2 \cos \alpha) / 2$.

3.2. Nonuniformly twisted traveling states

Here, we look for generic traveling waves. Substituting (9) in relations (1), (2) and expanding the kernel (3) with trigonometric identities, we obtain that

$$\frac{d\phi(\xi)}{d\xi} = \frac{1}{v} \left[\Omega - \text{Im} \left(h(\xi) e^{-i\phi(\xi) - i\alpha} \right) \right], \quad (13)$$

$$h(\xi) = \int_{-\pi}^{+\pi} G(\xi - \zeta) e^{i\phi(\zeta)} d\zeta = h_0 + h_1 \cos \xi + h_2 \sin \xi, \quad (14)$$

where the complex coefficients h_0 , h_1 and h_2 are given by

$$h_0 = \frac{1}{2\pi} \int_{-\pi}^{+\pi} e^{i\phi(\zeta)} d\zeta, \quad (15a)$$

$$h_1 = \frac{g_1}{2\pi} \int_{-\pi}^{+\pi} e^{i\phi(\zeta)} \cos \zeta d\zeta - \frac{g_2}{2\pi} \int_{-\pi}^{+\pi} e^{i\phi(\zeta)} \sin \zeta d\zeta, \quad (15b)$$

$$h_2 = \frac{g_1}{2\pi} \int_{-\pi}^{+\pi} e^{i\phi(\zeta)} \sin \zeta d\zeta + \frac{g_2}{2\pi} \int_{-\pi}^{+\pi} e^{i\phi(\zeta)} \cos \zeta d\zeta. \quad (15c)$$

Additionally, the boundary condition (10) should be fulfilled.

Next, we briefly describe the procedure for finding traveling waves with different spatial rotation numbers M . According to equations (13) and (14), at a glance, each phase profile $\phi(\xi)$ belonging to this class of nontrivial collective modes depends on eight unknown quantities Ω , v , h_0 , h_1 and h_2 (because h_0 , h_1 and h_2 are complex). However, only six conditions (15) of self-consistency are to be fulfilled. On the other hand, because of the phase shift invariance $\varphi \rightarrow \varphi + \varphi_0$ and the space shift invariance $x \rightarrow x + x_0$ (where φ_0 and x_0 are arbitrary constants), one can set (without loss of generality) the values h_0 and h_2 to be real. Therefore, we reduce the number of unknowns by two and arrive at the system of six nonlinear equation (15) for six real variables Ω , v , h_0 , $\text{Re}(h_1)$, $\text{Im}(h_1)$ and h_2 , where the trajectory $\phi(\xi)$ is calculated with the help of equation (13) and satisfies the condition (10).

For given values Ω , v , h_0 , h_1 and h_2 , equation (13) can be interpreted as the Adler equation with periodic coefficients in a nonlinear forcing term, where the structure of the complex function $h(\xi)$ is known explicitly from expression (14). For such an equation, the solution $\phi(\xi)$ satisfying the periodicity condition (10) can be reconstructed by using the related Poincaré map and its fix points (one of them is stable and the other is unstable). The corresponding Poincaré map coincides with the Möbius transformation that takes the closed unit disk onto itself [26–30]. According to [24, 30], the parameters of the canonical form of this transformation can be uniquely determined by employing two solutions of the supporting complex Riccati equation starting from the specific (specially selected) initial conditions. For fixed quantities Ω , v , h_0 , h_1 and h_2 , this approach allows one to obtain a periodic orbit for the phase variable $\phi(\xi)$ defined on a cylinder, which automatically meets the periodicity condition (10) and can be associated with the phase profile of the traveling wave we are looking for (see [24] for details).

As a result, for each set of the significant model parameters α , g_1 and g_2 , the problem of searching for a nonuniformly twisted state in the form of a continuous pattern with a permanent shape, moving at a constant velocity, reduces to the problem of detecting roots of equation (15), which can be solved numerically by a method based on the Newton–Raphson algorithm. A discussion of the details and subtleties (in particular, an iterative procedure for finding a good initial approximation close to the genuine roots of the nonlinear equations) of each stage of the developed procedure for constructing similar solutions in the model of oscillator lattices with advective–diffusive coupling can be found in the paper [24].

The robustness of traveling waves is evaluated as follows. To study the linear stability of the spatially inhomogeneous solutions obtained as described above, we, as the first step, rewrite the continuous AS model (1), (2) and (3) in the frame, rotating with frequency Ω and moving at speed v . In this reference frame, the nonuniformly twisted state is a stationary solution $\phi(\xi)$. Then, we represent $\varphi(\xi, t)$ in the form

$\varphi(x, t) = \phi(\xi) + \psi(\xi, t)$, where $\psi(\xi, t)$ describes ξ -periodic small deviations from the traveling wave profile $\phi(\xi)$. Substituting this expression into the basic equations for the phase variable, linearizing them in the vicinity of $\phi(\xi)$ and employing trigonometric identities, we arrive at the following linear integro-differential equation for $\psi(\xi, t)$ with coefficients independent of t :

$$\begin{aligned} & \frac{\partial \psi(\xi, t)}{\partial t} \\ &= v \frac{\partial \psi(\xi, t)}{\partial \xi} + \sin(\phi(\xi) + \alpha) \frac{1}{2\pi} \left[\int_{-\pi}^{+\pi} \psi(\zeta, t) \sin(\phi(\zeta)) d\zeta - \psi(\xi, t) \int_{-\pi}^{+\pi} \sin(\phi(\zeta)) d\zeta \right] \\ &+ \cos(\phi(\xi) + \alpha) \frac{1}{2\pi} \left[\int_{-\pi}^{+\pi} \psi(\zeta, t) \cos(\phi(\zeta)) d\zeta - \psi(\xi, t) \int_{-\pi}^{+\pi} \cos(\phi(\zeta)) d\zeta \right] \\ &+ (g_1 \sin \xi - g_2 \cos \xi) \sin(\phi(\xi) + \alpha) \frac{1}{2\pi} \left[\int_{-\pi}^{+\pi} \psi(\zeta, t) \sin \zeta \sin(\phi(\zeta)) d\zeta - \psi(\xi, t) \int_{-\pi}^{+\pi} \sin \zeta \sin(\phi(\zeta)) d\zeta \right] \\ &+ (g_1 \sin \xi - g_2 \cos \xi) \cos(\phi(\xi) + \alpha) \frac{1}{2\pi} \left[\int_{-\pi}^{+\pi} \psi(\zeta, t) \sin \zeta \cos(\phi(\zeta)) d\zeta - \psi(\xi, t) \int_{-\pi}^{+\pi} \sin \zeta \cos(\phi(\zeta)) d\zeta \right] \\ &+ (g_1 \cos \xi + g_2 \sin \xi) \sin(\phi(\xi) + \alpha) \frac{1}{2\pi} \left[\int_{-\pi}^{+\pi} \psi(\zeta, t) \cos \zeta \sin(\phi(\zeta)) d\zeta - \psi(\xi, t) \int_{-\pi}^{+\pi} \cos \zeta \sin(\phi(\zeta)) d\zeta \right] \\ &+ (g_1 \cos \xi + g_2 \sin \xi) \cos(\phi(\xi) + \alpha) \frac{1}{2\pi} \left[\int_{-\pi}^{+\pi} \psi(\zeta, t) \cos \zeta \cos(\phi(\zeta)) d\zeta - \psi(\xi, t) \int_{-\pi}^{+\pi} \cos \zeta \cos(\phi(\zeta)) d\zeta \right]. \end{aligned} \tag{16}$$

Further, following the standard procedure of stability analysis, we seek $\psi(\xi, t)$ in factorized form $\psi(\xi, t) = \text{Re}(\Psi(\xi)e^{\lambda t})$. With a spatial discretization, the linear integral operator (16) reduces to a matrix, eigenvalues λ of which can be found numerically. The reliability of such an approach is confirmed by the overlap of found eigenvalues for different discretizations (see spectrum examples in a more complicated situation in [24]).

Here we also mention that our key assumption of the above presented analysis is that the nontrivial collective modes in the form of traveling waves propagating at constant velocities can be associated with nonuniformly twisted states having continuous phase profiles. On the other hand, using the OA approach [6, 7], in the thermodynamics limit (where $N \rightarrow \infty$), one can reduce the problem to low-dimensional dynamical systems for coarse-grained complex order parameter $Z(x, t)$. In the corresponding analytical procedure, the acting field $H(x, t)$ is expressed directly in terms of $Z(x, t)$ with the help of convolution where the Lebegues integral over the phase distribution $\varphi(x, t)$ (generally speaking, nonsmooth) is transformed, by virtue of coarse-graining, to the Cauchy integral over the continuous (relatively smooth) profile $Z(x, t)$. Such a transition to the averaged description makes it possible to provide a link between the fundamental concepts of synchronization phenomenon and the theory of nonlinear wave structures. This observation is one of main findings of the papers [2, 3, 9]. Despite the above advantages and benefits of the OA approach, we do not employ such a reduction in the presented study. We perform our theoretical analysis and numerical simulations within the framework of the basic equations of the dynamics of phase oscillator and also use the self-consistency arguments allowing one to formulate an integro-differential equation for a phase profile of a nonuniformly twisted state. Because we are looking for traveling wave patterns, it is natural to suppose that the continuous medium of phase oscillators is in a filly coherent state, i.e. $|Z(x, t)| = 1$ at each point $x \in [-\pi, \pi]$ at any time t . In this case, we assume that the system under consideration possesses regimes of behaviors where all identical elements rotate synchronously with the frequency Ω and the spatial distribution of the dynamical variable $\varphi(x, t)$ is determined by a smooth function $\phi(\xi)$ of the traveling coordinate $\xi = x - vt$. Actually, in terms of the OA manifold, this smooth profile $\phi(\xi)$ is the inhomogeneous part of the phase of complex order parameter $Z(x, t)$ which absolute value is identically equal to unity, i.e. $Z(x, t) = e^{i\Omega t + i\phi(\xi)}$.

3.3. Traveling wave profiles and their stability

Here, we will present the outcomes of these calculations and examine the properties of the corresponding modes. If a solution to the problem (13)–(15), or an approximate solution, is already available for certain

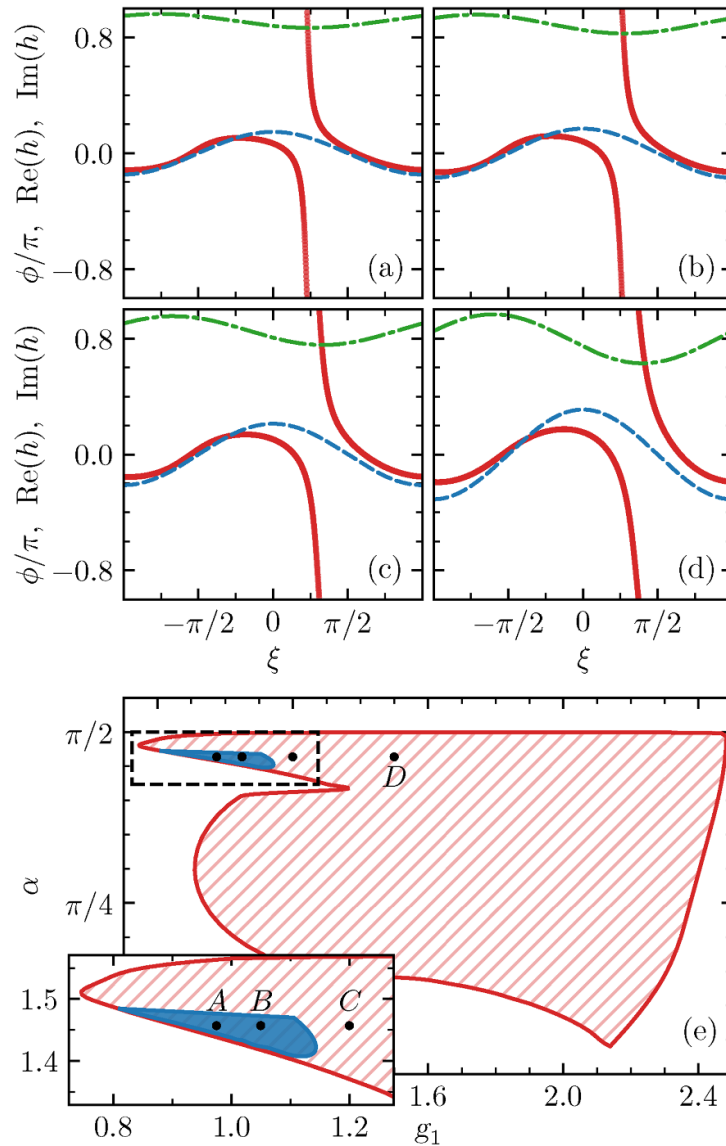


Figure 1. (a)–(d) Examples of traveling wave solutions with a spatial rotation number $M = -1$ which are found in the case of symmetric nonlocal interaction (i.e. $g_2 = 0$) for the phase lag $\alpha = 1.457$ and several values of g_1 : (a) $g_1 = 0.975$ (point A on panel (e)), (b) $g_1 = 1.05$ (point B on panel (e)), (c) $g_1 = 1.2$ (point C on panel (e)) and (d) $g_1 = 1.5$ (point D on panel (e)). The solid red line represents the phase profile $\phi(\xi)/\pi$ and the dash-dot green line depicts the real part of the complex mean field $h(\xi)$ determined by equations (14) and (15) and the dashed blue line is its imaginary part. (e) Regions (on the plane of parameters g_1 and α) of existence (area with red hatching) and stability (domain shaded in dark blue) of nonuniformly twisted states with $M = -1$ for the original AS model, where the coupling function is taken in the form (3) with $g_2 = 0$. The inset corresponds to the enlarged rectangular area outlined by the black dashed line.

values of α , g_1 and g_2 , then it becomes feasible to extend the solution to neighboring parameters. Of course, such a continuation is not possible for the integer winding number M . Consequently, for each fixed value of the phase shift number M , we obtain a family of traveling solutions with different velocities and rotation frequencies by continuation in the significant model parameters α , g_1 and g_2 .

3.3.1. Symmetric kernel

Let us begin with the standard symmetric AS setup, where $g_2 = 0$. Under this symmetric coupling condition, we have successfully identified traveling waves with spatial rotation numbers $M = \pm 1$ and $M = \pm 2$ exclusively. The phase profiles of the nonuniformly twisted states with $M = -1$ are depicted in panels (a)–(d) of figure 1. Additionally, figure 1(e) represents the parameter plane with axes g_1 and α , where we highlight the regions of existence and stability for the corresponding traveling wave solutions. It is evident from this figure that the existence region is quite extensive, whereas the stability domain is relatively small. In the stable domain, these nonuniformly twisted states can be observed during the long-term evolution of systems comprising a large number of oscillators. They may play a significant role in the nonequilibrium collective dynamics of ensembles of nonlocally interacting elements. Furthermore, in the vicinity of the stable domain,

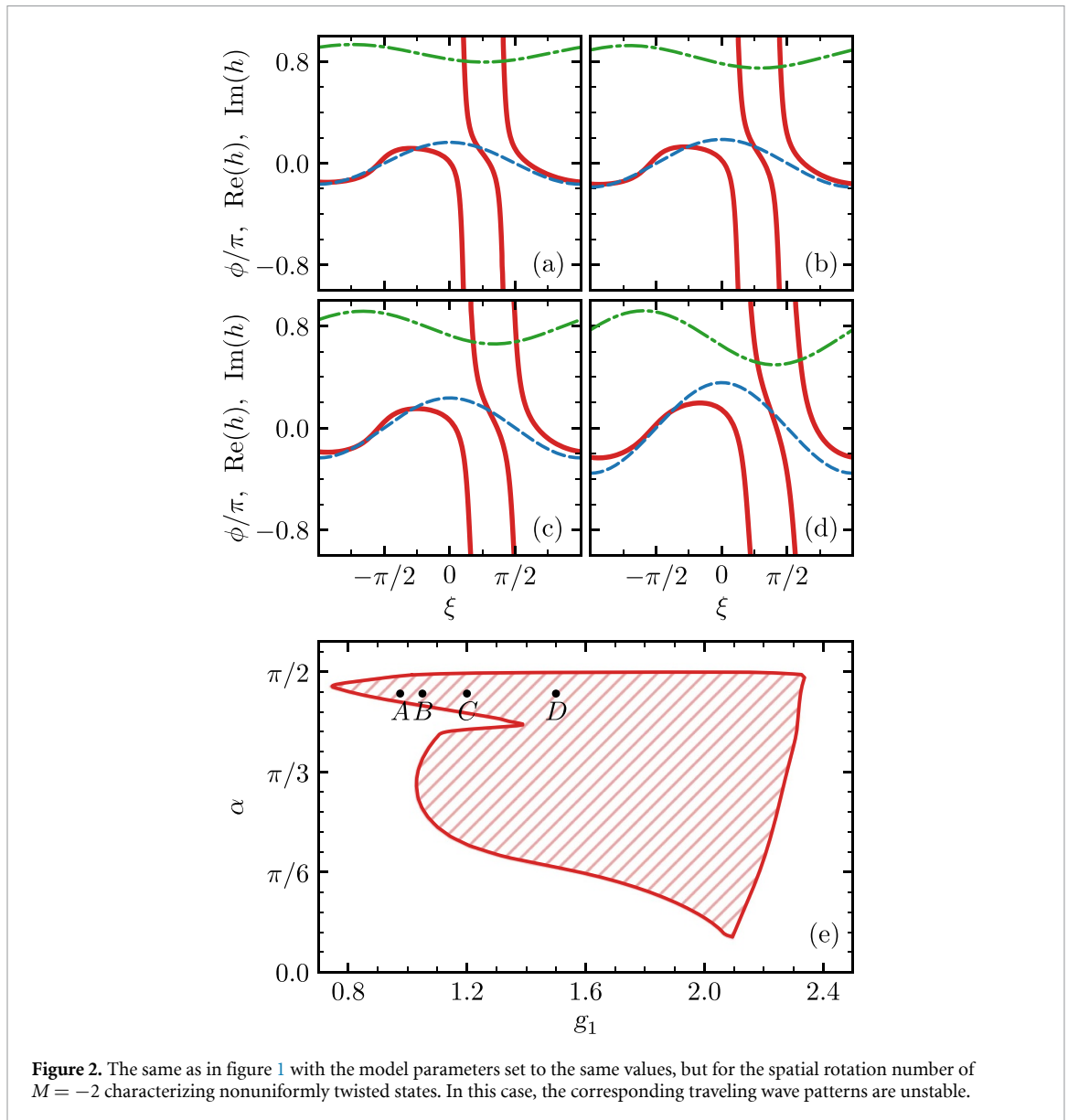


Figure 2. The same as in figure 1 with the model parameters set to the same values, but for the spatial rotation number of $M = -2$ characterizing nonuniformly twisted states. In this case, the corresponding traveling wave patterns are unstable.

a region exists where the traveling waves with $M = -1$ exhibit weak instability. Consequently, these waves may appear as transient states during the transition to complete phase synchrony or another (more complicated) collective mode.

Figures 2(a) and (d) display several examples of phase profiles for traveling wave solutions with $M = -2$ in the case of symmetric coupling. However, our analysis reveals that all of these wave patterns are unstable. The existence region of these unstable wave solutions is illustrated in figure 2(e).

3.3.2. Asymmetric kernel

Here, we consider asymmetric kernels with $g_2 \neq 0$. In figures 3 and 4, we present various examples and branches of solutions obtained for different values of the parameters M , α , g_1 and g_2 . To obtain these results, we employ a combination of the previously developed iterative procedure, which helps find an initial approximation for the solutions corresponding to a fixed spatial rotation number M (see appendix A in [24]), with the Newton–Raphson method for continuation along the asymmetry parameter g_2 of the coupling function (3) (see section 3.2). The findings demonstrate that this procedure allows exploring various nontrivial collective modes for integer values of $|M|$ ranging from one to large absolute values. For each set of α and g_1 values, the corresponding branch of traveling wave solutions is confined within certain limits of the asymmetry parameter g_2 .

Remarkably, the cases of $M = -1$ and $M = -2$ (and similarly $M = 1$ and $M = 2$) stand out from the rest. These cases allow the corresponding continuous phase profiles to exist not only for positive (negative) values of the asymmetry parameter g_2 but also for vanishing and even negative (positive) g_2 values. Of particular

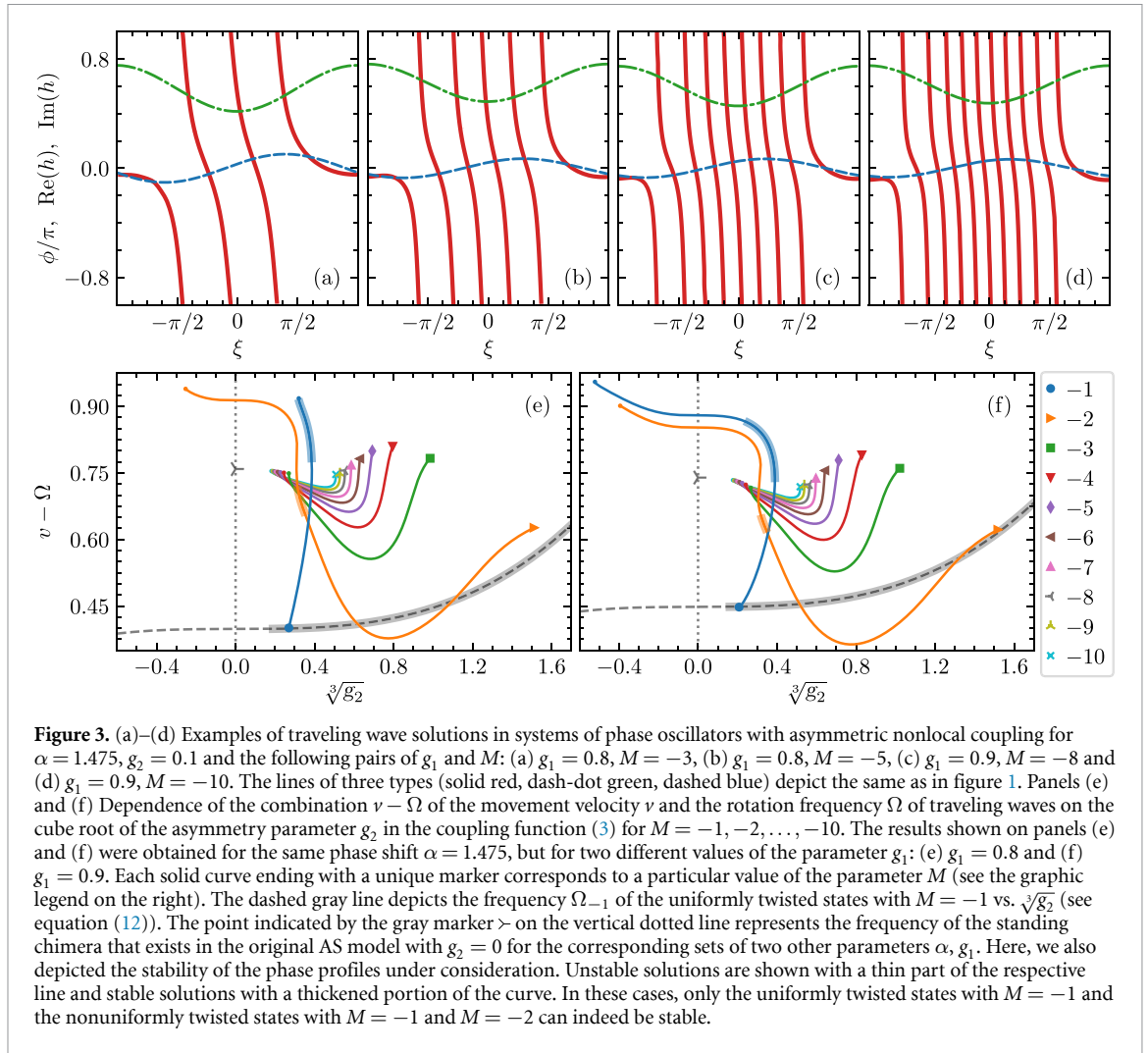


Figure 3. (a)–(d) Examples of traveling wave solutions in systems of phase oscillators with asymmetric nonlocal coupling for $\alpha = 1.475$, $g_2 = 0.1$ and the following pairs of g_1 and M : (a) $g_1 = 0.8$, $M = -3$, (b) $g_1 = 0.8$, $M = -5$, (c) $g_1 = 0.9$, $M = -8$ and (d) $g_1 = 0.9$, $M = -10$. The lines of three types (solid red, dash-dot green, dashed blue) depict the same as in figure 1. Panels (e) and (f) Dependence of the combination $v - \Omega$ of the movement velocity v and the rotation frequency Ω of traveling waves on the cube root of the asymmetry parameter g_2 in the coupling function (3) for $M = -1, -2, \dots, -10$. The results shown on panels (e) and (f) were obtained for the same phase shift $\alpha = 1.475$, but for two different values of the parameter g_1 : (e) $g_1 = 0.8$ and (f) $g_1 = 0.9$. Each solid curve ending with a unique marker corresponds to a particular value of the parameter M (see the graphic legend on the right). The dashed gray line depicts the frequency Ω_{-1} of the uniformly twisted states with $M = -1$ vs. $\sqrt[3]{g_2}$ (see equation (12)). The point indicated by the gray marker \triangleright on the vertical dotted line represents the frequency of the standing chimera that exists in the original AS model with $g_2 = 0$ for the corresponding sets of two other parameters α, g_1 . Here, we also depicted the stability of the phase profiles under consideration. Unstable solutions are shown with a thin part of the respective line and stable solutions with a thickened portion of the curve. In these cases, only the uniformly twisted states with $M = -1$ and the nonuniformly twisted states with $M = -1$ and $M = -2$ can indeed be stable.

interest, we observe that the branch of nonuniformly twisted states with $M = -1$ (and $M = 1$) intersects with the branch of uniformly twisted states of type (11) with $M = -1$ (and $M = 1$) at a certain point (for fixed values of α and g_1). A bifurcation occurs at the parameters corresponding to this junction of the specified branches. In section 3.1 we have shown that the uniformly twisted states existing in the considered model can have the winding number, which is equal only to unity in absolute value, i.e. $|M| = 1$. The states with larger winding number ($|M| > 1$) do not exist in the system under study. Therefore, bifurcations curves of nonuniformly twisted states with $|M| > 1$ do not intersect with those of uniformly twisted states because of their absence. In the case $|M| = 1$ (for fixed values of the phase lag α and the kernel parameter g_1), a bifurcation curve of a nonuniformly twisted state intersects with that of a uniformly twisted state. Approaching this point, the nonuniformly twisted state continuously transforms into the uniformly twisted state. The nontrivial traveling wave pattern converts into a trivial one. Such a situation is common and occurs for a set of pairs with different values of the phase shift α and the coupling kernel parameter g_1 . Thus, we have a two-dimensional surface in the three-dimensional space of system parameters corresponding to the considered bifurcation, so that this picture can be interpreted as a codimension-1 bifurcation.

At higher values of the winding number $|M| > 3$ (figure 4), we observe that the regions where traveling wave patterns exist shift towards smaller values of g_2 as $|M|$ increases. This means that traveling waves with larger numbers of phase rotations are found for smaller asymmetry parameters g_2 and have correspondingly smaller velocities. Remarkably, it is possible to find traveling waves for extremely small values of g_2 ; however, this requires considering profiles with a very large number of phase shifts $|M|$ (as seen in figure 4). In the case of a vanishing asymmetry parameter g_2 , which corresponds to the original AS model, the nonuniformly twisted states appear to convert into standard standing chimeras characterized by the coexistence of synchronous and asynchronous patches of oscillators. In other words, the standing chimera regimes can be interpreted as nonuniformly twisted states with an infinitely large spatial rotation number $|M|$. This interpretation is supported by the observation that the branches shown in figure 4(e) tend to converge to a point representing the frequency of uniform rotation of the phase of the complex order parameter in a

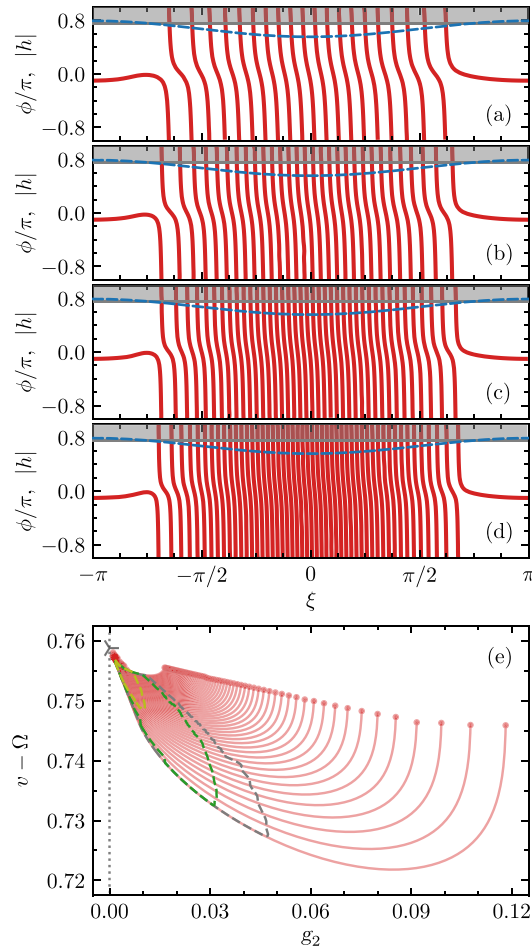


Figure 4. (a)–(d) Examples of traveling wave solutions in systems of phase oscillators with asymmetric nonlocal coupling for $\alpha = 1.475$, $g_1 = 0.8$ and the following values of g_2 and M : (a) $g_2 = 0.014$, $M = -20$, $\Omega = -0.7605$, $\nu = 0.0144$, (b) $g_2 = 0.014$, $M = -30$, $\Omega = -0.7584$, $\nu = 0.0096$, (c) $g_2 = 0.007$, $M = -40$, $\Omega = -0.7597$, $\nu = 0.0071$ and (d) $g_2 = 0.007$, $M = -50$, $\Omega = -0.7590$, $\nu = 0.0057$. The solid red line represents the phase profile $\phi(\xi/\pi)$ and the dashed blue line depicts the amplitude of the complex mean field $h(\xi)$. The gray line indicates the value $|\Omega|$ and the gray shaded area corresponds to the domain $|h(x)| > |\Omega|$. (e), (f) Dependence of the combination $\nu - \Omega$ of the movement velocity ν and the rotation frequency Ω of traveling waves on the asymmetry parameter g_2 in the coupling function (3) for larger absolute values of the phase shift number M than in figure 3(e): $M = -11, -12, \dots, -80$. The point indicated by the gray marker \triangleright represents the same as in figure 3(e). Three closed dashed lines nested in each other outline the contour of the regions, inside which the maximum possible value of the real parts of the eigenvalues of the problem (16) does not exceed 8×10^{-3} , 2×10^{-3} and 5×10^{-4} , respectively. The traveling wave solutions corresponding to the points lying inside the smallest of these three regions can be considered as quasi-stable transient states.

standard chimera regime. Note, in the symmetric case when $g_2 \rightarrow 0$ and $|M| \rightarrow \infty$, actually, the following transition takes place. The phase profiles in regions of partial synchrony become more and more steep. The characteristic spatial scale at which the phase changes by 2π should be compared with the spatial scale, adopted for the definition of the coarse-grained order parameter Z . In terms the OA manifold, this means the domains with $|Z(x, t)| < 1$ appear.

Before we briefly discuss the stability analysis results, it is essential to emphasize that we have not identified any particularly interesting transformation of traveling waves with each specific value of the spatial rotation number M along its corresponding branch. However, it is also worth noting that the phase profiles of the traveling wave solutions become increasingly sharp towards the ends of their domains of existence. Regrettably, this sharpness poses challenges when attempting to continue the discovered branches of solutions beyond the presented ranges.

As is depicted in panels (e) and (f) of figure 3, introducing an asymmetry in the coupling function results in stabilizing the uniformly twisted states with $|M| = 1$. Similarly, the nonuniformly twisted states with $|M| = 1$ and $|M| = 2$, which exist for $g_2 = 0$, become stable within finite ranges of g_2 . Throughout the explored parameter range ($0.3\pi \leq \alpha \leq 0.5\pi$, $0 \leq g_1 \leq 3$, $|g_2| \leq 0.5$), we have identified stable traveling waves only with $|M| = 1$ and $|M| = 2$. All traveling waves with larger winding numbers $|M|$ are found to be unstable. However, it is essential to note that among these states, some are only weakly unstable (with a maximum value of the

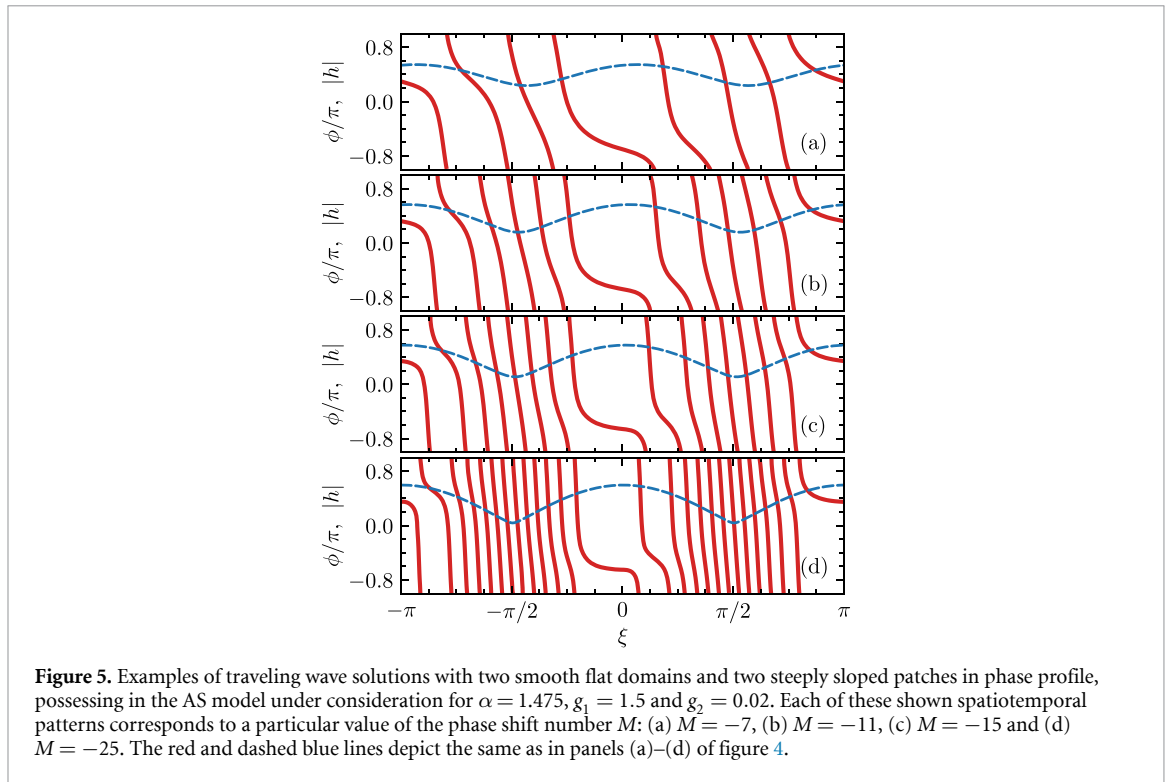


Figure 5. Examples of traveling wave solutions with two smooth flat domains and two steeply sloped patches in phase profile, possessing in the AS model under consideration for $\alpha = 1.475$, $g_1 = 1.5$ and $g_2 = 0.02$. Each of these shown spatiotemporal patterns corresponds to a particular value of the phase shift number M : (a) $M = -7$, (b) $M = -11$, (c) $M = -15$ and (d) $M = -25$. The red and dashed blue lines depict the same as in panels (a)–(d) of figure 4.

real part over the eigenvalue spectrum less than 5×10^{-4}). Consequently, these weakly unstable waves may appear as transient states, particularly during intermittency processes, to be described below.

Finally, we mention that the developed procedure enables the discovery of additional traveling wave solutions with more intricate continuous phase profiles. In particular, in figure 5, we demonstrate several examples of such traveling waves, each maintaining a fixed shape while moving at a constant velocity along an oscillatory medium closed in a ring. A distinctive feature of these solutions is the presence of two smooth flat domains and two steeply sloped patches in their phase profiles. These nontrivial collective modes can be closely associated with so-called ‘antiphase’ chimera states.

4. Dynamics of ensembles of phase oscillators

4.1. Evolution of traveling waves

Above, we focused on traveling waves within a continuous in space setup. Now, we delve deeper into the behavior of these modes in a finite population of N oscillators. In direct numerical simulations of a system of N ODEs (4)–(6), we commence with one of the exact traveling wave solutions found in the continuous limit, to which we introduce random perturbations ψ_n within the range $-d \leq \psi_n \leq d$.

4.1.1. Evolution of traveling waves with small spatial winding numbers

We start with solutions with small winding numbers $|M| \leq 7$ and focus on linearly stable traveling waves. In figure 6, we present the outcomes of direct numerical simulations within the symmetric coupling case ($g_2 = 0$), for a stable solution with $M = -1$. In each panel, two snapshots of the phase profiles are provided for two distinct values of the number of units in the system: $N = 128$ and $N = 1024$ (initial profiles have been additionally shifted for clarity of presentation). Panels (a)–(c) in figure 6 show that the small-amplitude random perturbations of magnitude $d = 0.02\pi$ added to an exact traveling wave solution at the initial moment $t = 0$ gradually dissipate over time and ultimately vanish. Consequently, the regular traveling wave re-emerges (see figures 6(c) and (e)) and persists over a large time interval (specifically $T = 5 \times 10^5$). These simulations confirm the robustness of this traveling wave in the discrete setting. However, if the strength d of the random perturbation exceeds a critical threshold value d_* ($d_* \approx 0.025\pi$ for the case depicted in figure 6), the traveling wave pattern undergoes disruption. This leads to its transition into a standing chimera state or, in some cases, to a homogeneous synchronous state. On the other hand, it is worth mentioning that, under certain conditions, unstable uniformly twisted states with $|M| = 1$ evolve into stable traveling wave solutions, which appear as unevenly twisted states with $|M| = 1$ can be essentially interpreted as quasiperiodic coherent states [31].

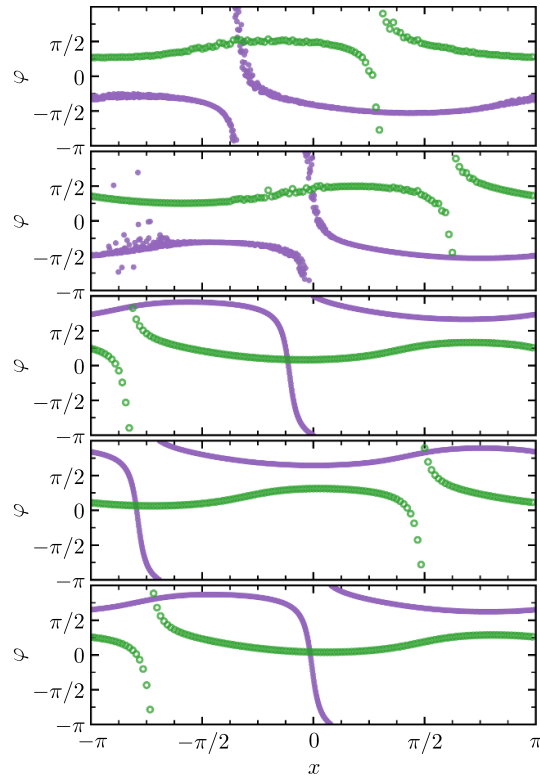


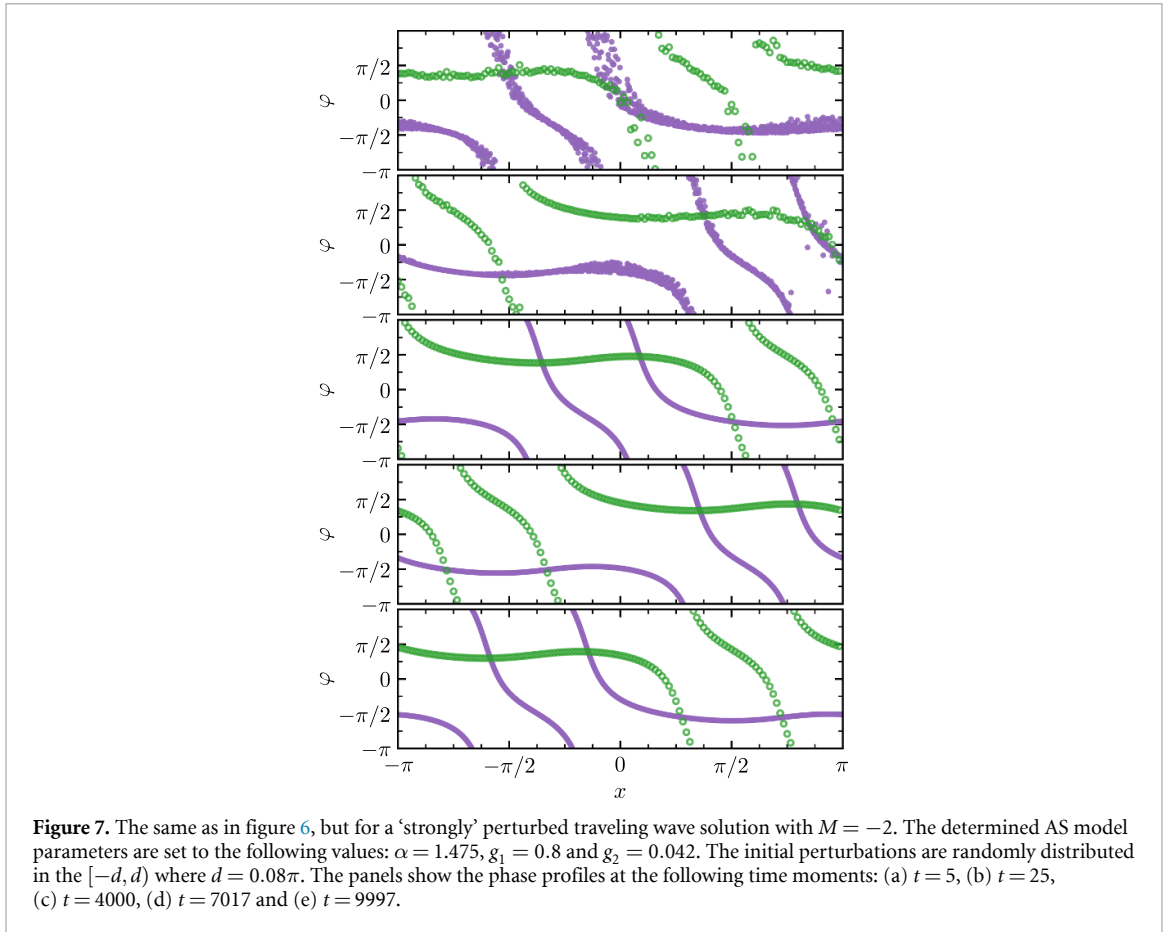
Figure 6. Evolution of a ‘slightly’ perturbed numerically found traveling wave solution with $M = -1$ in simulations of the lattice equations (4), (6) and (3) for the phase lag $\alpha = 1.457$ and parameters $g_1 = 1.05$ and $g_2 = 0$. The perturbations ψ_n added to the exact traveling wave solution $\phi_n = \phi(x_n)$ obey a uniform distribution in the interval $[-d, d]$ where $d = 0.02\pi$. The dotted violet lines merging into a solid curve represent the phase profiles $\varphi_n(t) = \varphi(t, x_n)$ for the case $N = 1024$. The green unshaded circles depict the instantaneous phases $\varphi_n(t)$ for the number of elements $N = 128$ at the following time moments: (a) $t = 5$, (b) $t = 25$, (c) $t = 4500$, (d) $t = 7000$ and (e) $t = 10\,000$. The oscillators are placed at equidistant points $x_n = \pi(2n - N)/N$ in the spacial domain of length $\ell = 2\pi$. All snapshots of phase distributions are shown in the reference frame rotating with the frequency Ω of the corresponding exact traveling wave solution.

In cases involving asymmetric coupling ($g_2 \neq 0$), the persistence of nontrivial traveling waves endures across a wide range of noise strengths d . This phenomenon is prominently displayed in figure 7, where we conduct direct numerical simulations to illustrate the propagation of a perturbed traveling wave solution with $M = -2$. Here, the initial random perturbation is $d = 0.08\pi$. The key findings and primary conclusions align with those expounded above: an ordered profile emerges and the discrete phase distribution repeatedly runs over the system without altering its shape when viewed from the appropriately chosen reference frame. It is worth noting that, for the sake of clarity of presentation, the phase profiles showcased in both figures 6 and 7 are depicted in the reference frame that rotates at the frequency Ω corresponding to the exact traveling wave solution for each respective situation. Panels (c)–(e) in these figures unequivocally demonstrate that, in both cases, the phase profiles exhibit uniform rotation at the frequency Ω , thereby conforming the establishment of the exact traveling wave solution in the form of an unevenly twisted synchronized state.

Numerical simulations starting with an unstable traveling wave solution characterized by relatively small (in magnitude) winding numbers $|M| \leq 7$ (not shown) demonstrate disruption through a cascade of transformations. As a result, in the case of symmetric coupling ($g_2 = 0$), such modes evolve into standing standard chimeras or into fully synchronous states. Alternatively, under certain conditions, they may also evolve into uniformly twisted states with $|M| = 1$ when $g_1 > 1$. In contrast, in scenarios involving asymmetric coupling ($g_2 \neq 0$), the potential outcomes are restricted to the emergence of regular modes, such as fully synchronous regimes or twisted states.

4.1.2. Evolution of traveling waves with large winding numbers into weakly turbulent traveling chimeras

Here, we describe a typical scenario observed when employing direct numerical simulations involving a slightly asymmetric coupling function from an initial perturbed profile of one of the exact traveling wave solutions with multiple continuous branches (characterized by large winding numbers M). The main observation, illustrated in figure 8, is that on a long time scale, the profile becomes disordered, albeit not completely and thus will be termed ‘traveling chimera’.



Figures 8(a) and (b) illustrate that during the initial transient phase of the evolution process (roughly one rotation around the ring), the noise within the initially randomly disturbed phase profile is substantially suppressed. While some slight deviations from an ordered phase profile are still discernible in figure 8(b), the random perturbations introduced to the exact traveling wave solution at the initial time moment $t = 0$ almost entirely vanish and become nearly imperceptible (at least through visual inspection of figures 8(c) and (d)). At the intermediate time range (several rotations of the wave around the circle), the evolution is similar to the stable cases presented in figures 6 and 7. Figures 8(c) and (d) depict phase distributions that closely resemble each other but are shifted along the circle. Nonetheless, this phase profile exhibits weak instability, eventually leading to the development of modulations. Distances between certain branches decrease while others increase (as seen in figures 8(e) and (f)). This irregular modulation process promotes the merging and disappearance of some branches. Consequently, in the later stages, the once-regular structure of the traveling wave pattern undergoes partial disruption and, following a prolonged transient, evolves into a turbulent state. We term this regime ‘weak turbulence’ due to its inherently irregular nature, which, nevertheless, largely retains the appearance of a locally continuous phase profile, at least in most regions (particularly in dense systems with a substantial number of elements N). Thus, this term aptly describes the evolving collective dynamics depicted in figures 8(e) and (f). It is worth noting that for a fixed set of determining parameters α , g_1 and g_2 of the generalized AS model, this particular collective mode emerges across various values of the strength d governing the random perturbations ψ_n introduced at the initial time moment. This parameter primarily influences the characteristic transition times: a larger d results in a longer time interval for the formation of a profile closely resembling the traveling wave solution discussed in section 3.3, but it becomes unstable more rapidly compared to scenarios when a smaller noise strength δ is employed.

The images presented in figures 8(e) and (f) possess a strong inhomogeneity: at each snapshot, there is a domain where the neighbors are synchronized (smooth profile of phases) and a domain where this smoothness is lost. In the latter disordered domain, one can still see at some places nearly continuous steep profiles if the density of oscillators is large (large N). Still, such domains appear nearly fully disordered for small densities (we will quantitatively characterize this in section 5). Hence, we classify this evolving nontrivial collective mode as a ‘traveling chimera’. It is worth highlighting that this term has previously

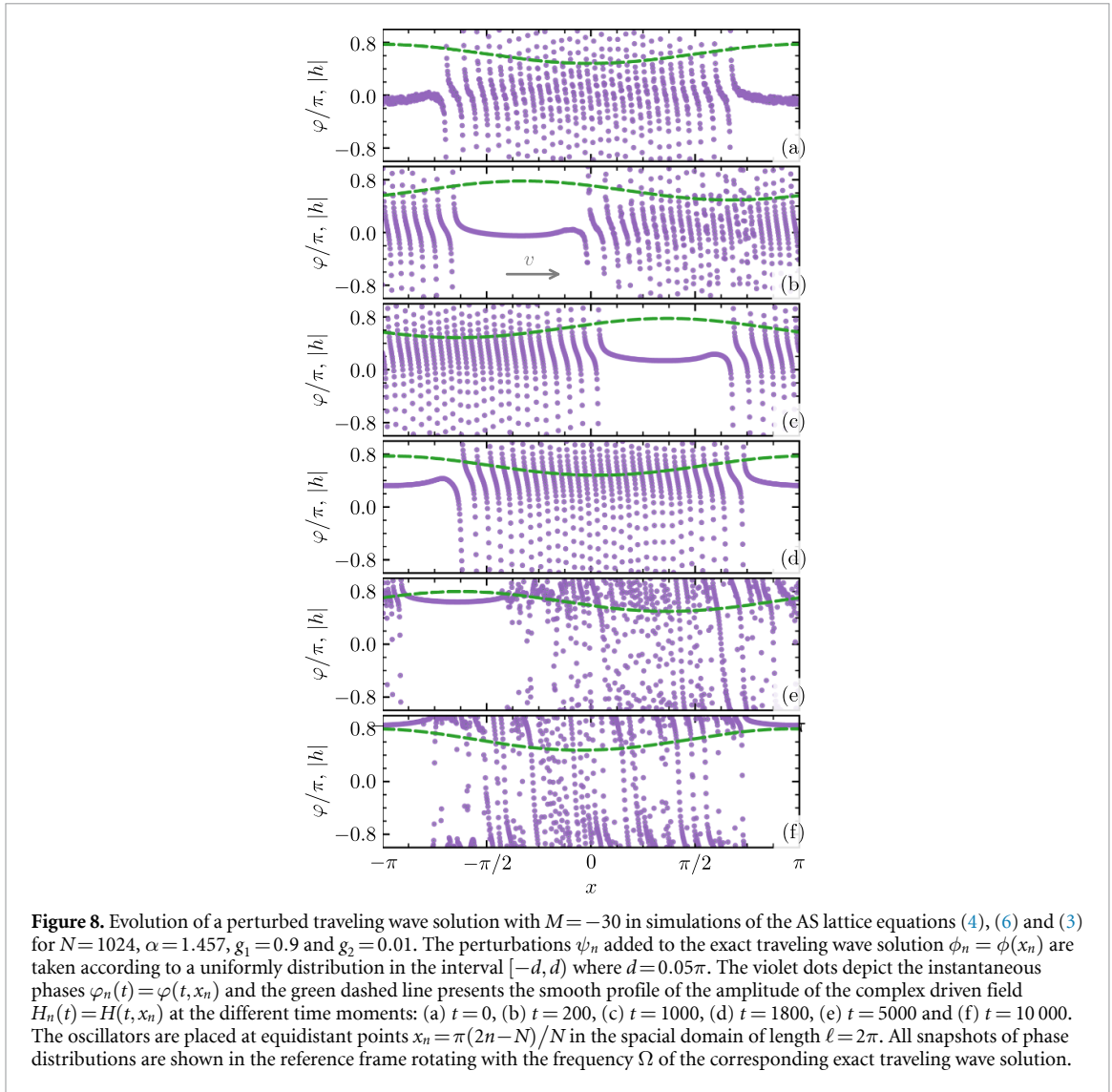


Figure 8. Evolution of a perturbed traveling wave solution with $M = -30$ in simulations of the AS lattice equations (4), (6) and (3) for $N = 1024$, $\alpha = 1.457$, $g_1 = 0.9$ and $g_2 = 0.01$. The perturbations ψ_n added to the exact traveling wave solution $\phi_n = \phi(x_n)$ are taken according to a uniformly distribution in the interval $[-d, d]$ where $d = 0.05\pi$. The violet dots depict the instantaneous phases $\varphi_n(t) = \varphi(t, x_n)$ and the green dashed line presents the smooth profile of the amplitude of the complex driven field $H_n(t) = H(t, x_n)$ at the different time moments: (a) $t = 0$, (b) $t = 200$, (c) $t = 1000$, (d) $t = 1800$, (e) $t = 5000$ and (f) $t = 10000$. The oscillators are placed at equidistant points $x_n = \pi(2n - N)/N$ in the spatial domain of length $\ell = 2\pi$. All snapshots of phase distributions are shown in the reference frame rotating with the frequency Ω of the corresponding exact traveling wave solution.

appeared in the literature [23, 24], describing regimes closely related to the modes discussed in this section.

Within all the snapshots of phases $\varphi_n(t) = \varphi(t, x_n)$ presented in figure 8, we also provide profiles of the absolute value of the driving field $|H_n(t)| = |H(t, x_n)|$. These profiles appear notably smooth across all instances due to coarse-grained averaging. Remarkably, the maximum of the driving field $|H(t, x_n)|$ resides within the mostly synchronous domain, where phases exhibit proximity to one another, forming an almost horizontal bar. This characteristic aligns with one of the distinctive features of chimera states. In particular, for the classical standing chimeras, the complex field $H(t, x_n)$ amplitude reaches maximums within the synchronous regions and minimums within the disordered domains. Furthermore, within the AS system of nonidentical phase oscillators with nonlocal asymmetric coupling, previous studies [13, 14, 25] have demonstrated that synchronization wave patterns moving at constant velocities, termed ‘traveling chimeras’ in these papers, represent the prevalent nontrivial collective modes. In this context, the phase profile consistently remains disordered, but the driving field $H(x, t)$ displays inhomogeneity, featuring both a maximum and a minimum while moving along the system closed in a ring. The regimes described in our current work are typified by a moving inhomogeneous profile of the complex mean field $H(x, t)$, akin to the concept of ‘traveling chimeras’ introduced in [13, 14, 25]. Hence, the modes we elucidate notably resemble classical chimera states, particularly in discrete systems with a relatively small number of elements. Thus, the term ‘traveling chimera’ proves apt in the present context. However, we emphasize once more that the key distinction lies in the mobility of domains along the lattice. The primary contrast with symmetric chimera states emerges in the partially synchronous domains surrounding the principal synchronous zone. In the case

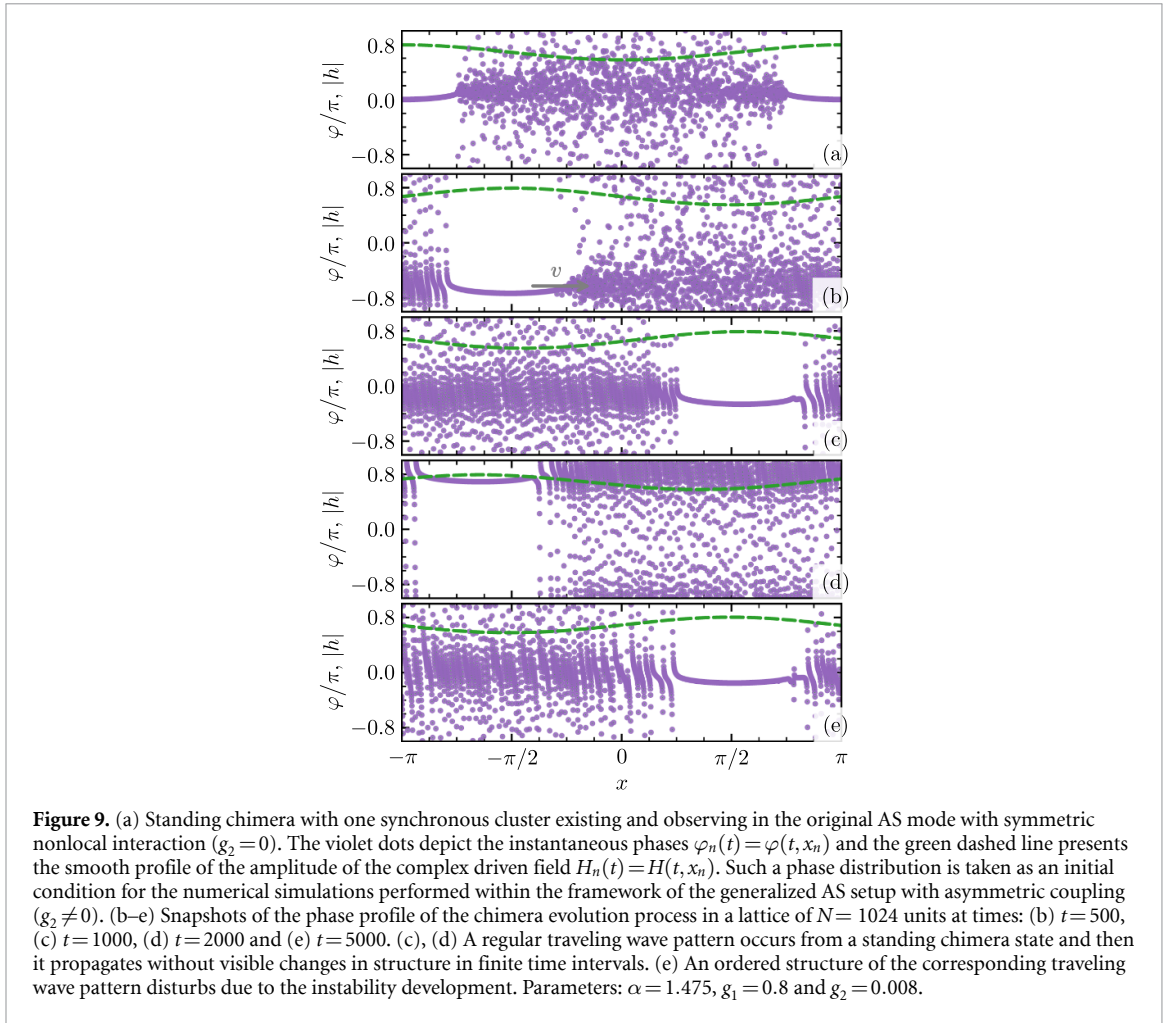


Figure 9. (a) Standing chimera with one synchronous cluster existing and observing in the original AS mode with symmetric nonlocal interaction ($g_2 = 0$). The violet dots depict the instantaneous phases $\varphi_n(t) = \varphi(t, x_n)$ and the green dashed line presents the smooth profile of the amplitude of the complex driven field $H_n(t) = H(t, x_n)$. Such a phase distribution is taken as an initial condition for the numerical simulations performed within the framework of the generalized AS setup with asymmetric coupling ($g_2 \neq 0$). (b–e) Snapshots of the phase profile of the chimera evolution process in a lattice of $N = 1024$ units at times: (b) $t = 500$, (c) $t = 1000$, (d) $t = 2000$ and (e) $t = 5000$. (c), (d) A regular traveling wave pattern occurs from a standing chimera state and then it propagates without visible changes in structure in finite time intervals. (e) An ordered structure of the corresponding traveling wave pattern disturbs due to the instability development. Parameters: $\alpha = 1.475, g_1 = 0.8$ and $g_2 = 0.008$.

of identical elements with nonlocal asymmetric coupling, these domains exhibit a significant level of coherence among oscillators, although they do not reach perfect synchronization.

4.2. Evolution of initial standing chimera states

Here, we explore evolution in a finite ensemble, starting with standard standing chimera states with one or two synchronous domains [3, 32] existing at vanishing asymmetry $g_2 = 0$. We prepare these initial conditions and demonstrate their evolution at $g_2 \neq 0$ in figures 9 and 10. Panels (a) at these figures show the initial states. Panels (b)–(e) demonstrate a transformation of standing chimeras into traveling chimeras.

At the first stage, after switching on the asymmetry in the coupling, the initial phase distribution starts to move (figures 9(b) and 10(b)). Behind the moving coherent domain, the phases become more correlated; they form steep, relatively smooth profiles. After one revolution of the coherent domain, the overall pattern resembles the exact traveling wave profiles constructed above. However, the same instability as has been discussed in section 4.1.2 leads to weakly turbulent regimes (panels (e)). This illustrates that the weakly turbulent moving chimera appears both from an initial exact traveling wave and from an initial standing chimera.

Numerical simulations on a long time interval $T = 5 \times 10^5$ show that the traveling chimera regime emerging from the classical standing chimera always survives only for small values of the asymmetry parameter g_2 . (The inferences given here assume that g_2 is positive, but it is also easy to generalize to negative values of the parameter g_2 .) For a fixed set of other determining parameters α and g_1 the AS model, there is a specific range of values g_2 for which only for a part of all runs the moving weakly turbulent state is also preserved at the time moment when simulations stopped and for another part of all runs the traveling chimeras decay and transform to the homogeneous synchronous mode. For g_2 values lying in a subsequent bounded range, the traveling chimera state is a long transient, after which a regular state arises.

Noteworthy, the observed situations where traveling chimera states are long transients should be juxtaposed with similar observations for standard chimeras (at $g_2 = 0$). This regular state can be either a fully synchronous state where all the phases are equal or a uniformly twisted wave with $|M| = 1$ where all the

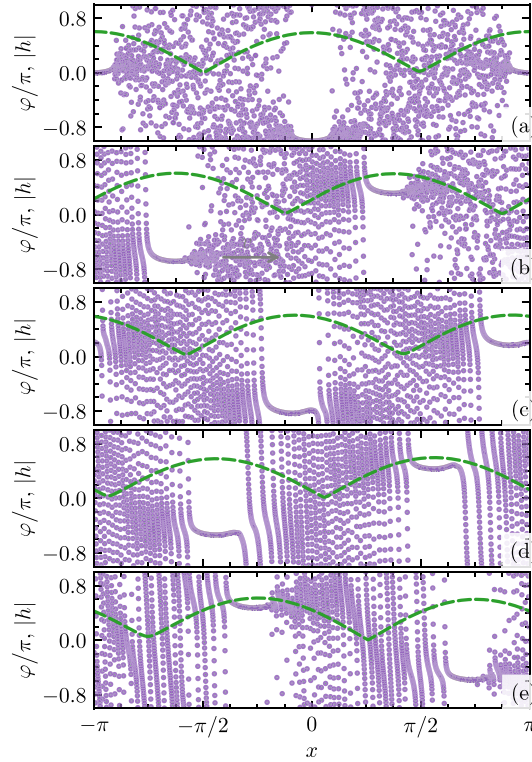


Figure 10. The same as in figure 9, but for the case where the numerical simulations start from a standing chimera with two antiphase synchronous clusters (panel (a) $t=0$) as an initial condition. (b–e) Chimera states at different moments of time in a lattice of $N=1024$ units: (b) $t=500$, (c) $t=1000$, (d) $t=2000$ and (e) $t=5000$. Parameters: $\alpha=1.475$, $g_1=1.5$ and $g_2=0.001$.

phases form a linear spatial profile or a nontrivial regular traveling wave with $|M|=1$ or $|M|=2$. In the second range, the dominant asymptotic regime is a uniformly twisted wave with $|M|=1$. As values of the asymmetry parameter g_2 increase, a synchronous state is more likely to emerge after a relatively short characteristic transient time. Here, we restrict ourselves to such a qualitative description of the results. However, the more detailed analysis and quantitative study of a similar evolution process can be found in the paper [24] where were reported a statistical evaluation of the fate of an initial standing classical chimera in the KB model of a phase oscillator lattice with advective-diffusive coupling. We additionally mention that, in the case of the AS setup, as in the generalized KB model, we have not found any significant dependence of the characteristic lifetimes of traveling turbulent chimeras on the number of units N .

5. Characterization of traveling chimera

This section presents several quantitative characterizations of the traveling weakly turbulent chimeras.

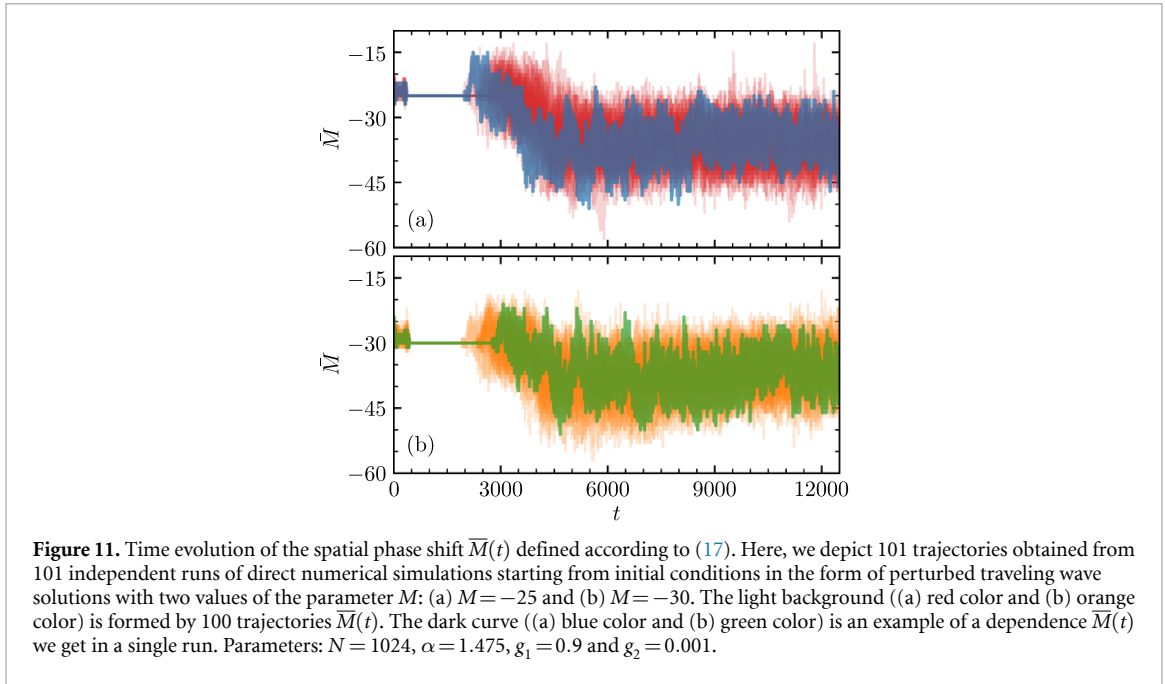
5.1. Number of phase slips

We have seen that at some stages of the evolution, the spatial phase profile can be considered as continuous (although we have a discrete lattice), see figures 8(c) and (d), while at other stages this continuity is at least partially broken, see figures 8(e) and (f). Continuous profiles have a definite winding number M , while this number is not well-defined for broken profiles. Nevertheless, we introduce an ‘empirical number of phase slips’ \bar{M} according to

$$\bar{M}(t) = \frac{1}{2\pi} \sum_{n=1}^{N-1} \arg \left[e^{i(\varphi_{n+1} - \varphi_n)} \right]. \quad (17)$$

For relatively smooth profiles, where $|\arg[e^{i(\varphi_{n+1} - \varphi_n)}]| \ll 1$, the phase shift $\bar{M}(t)$ is reliably determined and coincides with the winding number (8). Importantly, we will also apply expression (17) to erratic profiles even though the phase shift along the spatial domain cannot be unambiguously defined in such cases.

Figure 11 showcases the temporal evolution of the phase shift $\bar{M}(t)$ obtained through direct numerical simulations. These simulations start from initial conditions represented by randomly perturbed traveling wave solutions, featuring two different values of the parameter M : $M=-25$ (panel (a)) and $M=-30$



(panel (b)). Noteworthy, at the initial time $t=0$, the phase shift $\bar{M}(t=0)$ is not precisely defined, primarily due to the influence of added random perturbations ψ_n with a strength of $d = 0.05\pi$. Evidently, during the initial phase, while the ordered discrete phase profile is still forming, the phase shift $\bar{M}(t)$ fluctuates over time. This behavior directly reflects the inherent non-smoothness within the phase profile. Subsequently, as the relatively regular profile emerges (similar to the depiction in figures 8(b)–(d)), the value of $\bar{M}(t)$ stabilizes and becomes well-defined, exhibiting no further fluctuations. Over an extended duration, the phase shift $\bar{M}(t)$ remains nearly constant, with values of $\bar{M}(t) \approx -25$ (top panel) and $\bar{M}(t) \approx -30$ (bottom panel), respectively. However, this state is weakly unstable, ultimately leading to the development of a weakly turbulent state. In the later stages, the collective dynamics is characterized by the coexistence of synchronous macroscopic groups of oscillators featuring approximately identical phases alongside localized regions of spatiotemporal intermittency. Thus, the phase shift $\bar{M}(t)$ loses its well-defined nature, undergoing substantial changes during its evolution. The discernible fluctuations observed within the dependence $\bar{M}(t)$ on a small timescale indicate the presence of non-smooth phase variations, with such small non-smooth domains readily visible in figures 8(e) and (f). Notably, for a fixed set of AS model parameters, this chaotic collective mode remains statistically consistent across initial conditions characterized by perturbed traveling wave solutions with different values of M ($|M| > 7$). Furthermore, these small-scale fluctuations coexist in each trajectory with more pronounced long-scale variations. In figure 11, the observed long time scale fluctuations are not particularly large, but their magnitude grows with the increasing asymmetry parameter g_2 . It is conceivable that, at higher values of g_2 , these expanded fluctuations could potentially lead to the eventual demise of the traveling chimera state, which can be interpreted as the ‘traveling chimera death’.

5.2. Mean velocity

Here and in the following subsections, we discuss properties of weakly turbulent states (in particular, using statistical methods). To illustrate our findings, we use the results of direct numerical simulations within the AS model (4), (6) and (3) for $\alpha = 1.521$, $g_0 = 1$, $g_1 = 0.75$ and various values of g_2 and different number of units N .

In figure 12, we show the mean velocity v of the traveling chimera states in dependence on the asymmetry parameter g_2 of the AS coupling function (3) for different number of units N . This quantity was determined numerically according to the position of the maximum of the acting field $|H(t, x_n)|$, which is rather smooth and, at each moment of time, has a spatial profile with only several extremes. Remarkably, the velocity v is proportional to the asymmetry parameter g_2 for its small values: $v \sim g_2$. Large statistical fluctuations at $g_2 \gtrsim 0.015$ reflect the fact that macroscopic fluctuations of the weak turbulence become larger at large asymmetry, leading to rather short lifetimes of chimeras.

5.3. Cross-correlations

As discussed above, in a weakly turbulent regime, there is a certain degree of continuity in the phase profiles, even in the disordered domain (in the ordered domain, the profile is evidently continuous). Thus, contrary

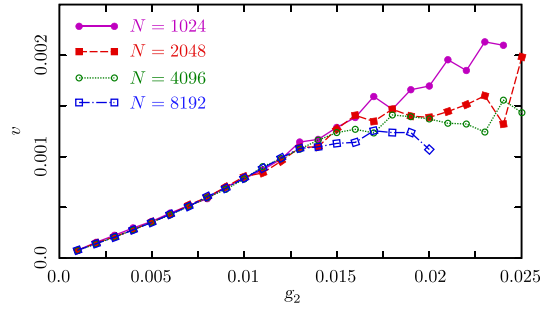


Figure 12. Dependence of the mean velocity of the traveling chimera state on the asymmetry parameter g_2 of the AS coupling function (3) for different number of units N . Other determining parameters of the AS lattice model: $\alpha = 1.521$ and $g_1 = 0.75$.

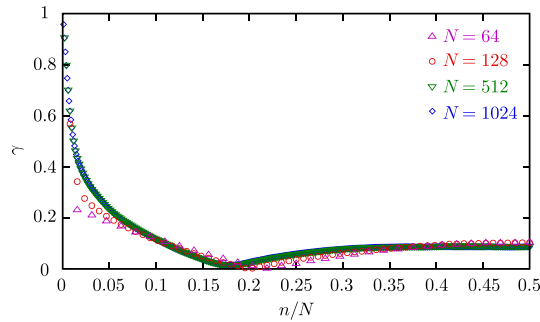


Figure 13. Correlation functions for different number of ensemble elements: $N = 64$ (magenta up-facing triangles), $N = 128$ (red circles), $N = 512$ (green down-facing triangles) and $N = 1024$ (blue diamonds). Determining parameters of the lattice AS system: $\alpha = 1.521$, $g_1 = 0.75$ and $g_2 = 0.02$.

to the standard standing chimera, where neighboring phases in the disordered domain are statistically independent (see figure 9(a)), here, there is a certain correlation between neighboring phases.

To characterize it quantitatively, we calculated the cross-correlation function of the phases. Because the phases are distributed nonuniformly, it is appropriate to use a transformation to nearly uniformly distributed phases $\varphi_n \rightarrow \vartheta_n$. For this, the global Kuramoto order parameter $\mathcal{Z}(t)$ is evaluated by the applying integration of the local order parameter $Z(x, t)$ over the entire medium (see section 2.2) and a Möbius transform is performed: $e^{i\vartheta_n} = (e^{i\varphi_n} - \mathcal{Z}) / (1 - \mathcal{Z}^* e^{i\varphi_n})$. After this, the quantity $\gamma(n) = \langle e^{i(\vartheta_n - \vartheta_{n+n})} \rangle$, where the brackets denote averaging in time and space, is calculated. The correlation function shown in figure 13 is $|\gamma(n)|$ versus normalized distance n/N for several values of the number N of elements. For large N , the correlation function tends to one at small distances, indicating local coherence and continuity of the phase profiles. In other words, the more dense the elements, the more visible the coherence between them. This reflects an average of significant correlations both in regular and in turbulent domains. However, we stress here again that the regimes which we describe for a relatively small number of oscillators indeed share almost all properties with chimera states in the classical sense, e.g. as one can see from figure 13, correlation of neighbors for $N = 64$ is close to 0.2.

5.4. Lyapunov exponents

Because the system's dynamics is purely deterministic, weak turbulence should be classified as spatiotemporal chaos in the system. Thus, it is natural to characterize it with the Lyapunov exponents [33]. The Lyapunov exponents calculated for a standard standing chimera and for a traveling weakly turbulent chimera state are presented in figure 14. The protocol of the calculations was as follows. First, an initial chimera-like profile of phases was created and integrated during the transient time 10^3 to achieve a statistically stationary state. Then, for calculation of the Lyapunov exponents, the time interval $5 \cdot 10^5$ was used, preceded by an additional transient time $5 \cdot 10^4$, during which the Lyapunov vectors are expected to be adjusted.

In figure 14(a), one can see the Lyapunov spectrum for a standard standing chimera (symmetric coupling $g_2 = 0$). A significant negative part corresponds to synchronous oscillators locked by the acting field $H_n(t)$. Then, there is a large number of nearly zero Lyapunov exponents, respectively, corresponding to oscillators in the disorder domain where their dynamics is nearly quasiperiodic. Additionally, there are a few positive Lyapunov exponents. Hence, in the case of symmetric coupling, a chimera state is weakly chaotic, as has been

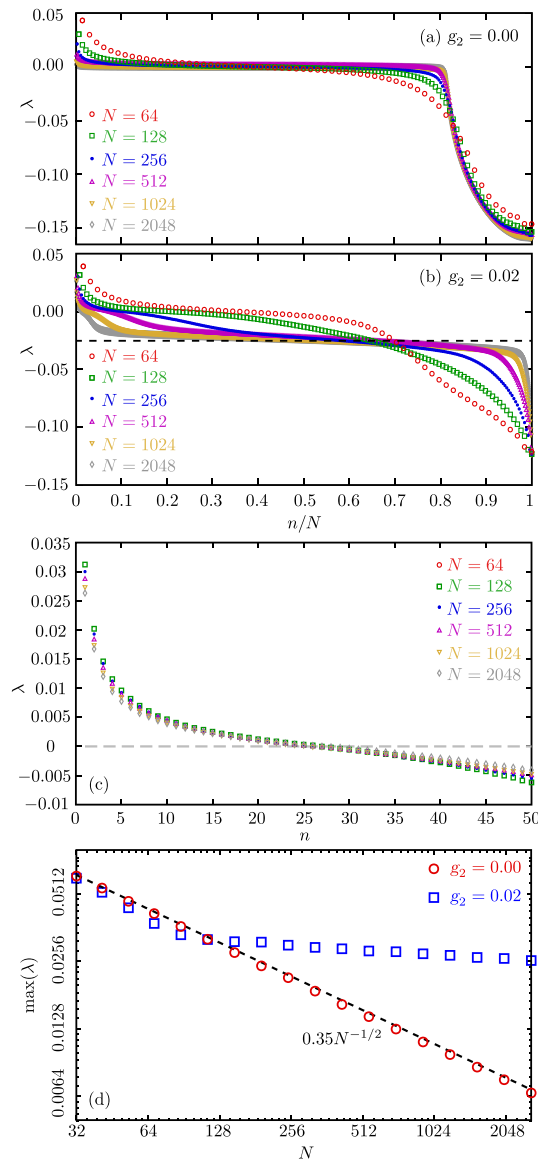


Figure 14. (a) Spectra of Lyapunov exponents λ for the standard standing chimera ($g_2 = 0$) for different numbers N of elements in the system. (b) Spectra of Lyapunov exponents λ for the traveling chimera state ($g_2 = 0.02$) for different numbers N of elements in the system. (c) The same as in the panel (b) but not in scaled coordinates. (d) Largest Lyapunov exponents for the standard standing chimera ($g_2 = 0$, red circles) and for traveling turbulent chimera ($g_2 = 0.02$, blue squares) depending on the number of units N . The dashed line is the power law $\sim N^{-1/2}$. Other determining parameters of the AS lattice model: $\alpha = 1.521$ and $g_1 = 0.75$.

discussed in [34–36]. However, in the thermodynamic limit (i.e. $N \rightarrow \infty$), the field $H(x, t)$ acting on oscillators is stationary (in the corresponding rotating reference frame). The Lyapunov exponents of particular oscillators are either negative (in the synchronous domain) or precisely zero (in the asynchronous domain). In figure 14(c), one can see that the largest (positive) Lyapunov exponent decays as $\sim N^{-1/2}$ with the number of elements in the system and tends to zero for $N \rightarrow \infty$. This indicates the absence of chaos in the thermodynamic limit $N \rightarrow \infty$.

The spectrum of Lyapunov exponents for traveling chimera with localized weakly turbulent domains (symmetric coupling $g_2 \neq 0$) is less trivial, see figure 14(b). First, because the pattern travels along the lattice, we cannot attribute particular Lyapunov exponents to particular oscillators. The next observation is that the profile of the Lyapunov spectrum changes quite significantly in the range $64 \leq N \leq 256$ and even for $512 \leq N \leq 2048$, we do not see an overlap, although qualitative features of the spectrum are quite similar. This absence of an overlap indicates that the spatio-temporal chaos is not extensive, at least with regard to parameter N at a fixed length of the system. To better visualize this, we show in figure 14(c) the same data vs. non-scaled index n . Here, one observes a good overlap (cf the N -dependence of the maximal Lyapunov exponent on N , shown in Figure 14(c); in contradistinction to the symmetric case $g_2 = 0$ it saturates at large values of N). This means that macroscopic chaos can be characterized by ≈ 25 positive Lyapunov exponents,

independent of the total number of oscillators N . The third distinctive feature is that a large number of Lyapunov exponents are concentrated around value ≈ -0.0253 (dashed line in panel (b)). This is the value of the transversal Lyapunov exponent, calculated from a perturbation of a single oscillator in a given fluctuating field $H(x_n, t)$. Because of ergodicity (due to the motion of the chimera), this value is the same for all oscillators. This negative value can be attributed to the observed correlations between the neighbors: because the dynamics of an oscillator in the driving field H is on average stable, close oscillators that feel close external fields have close states.

Altogether, exploring the Lyapunov exponents allows for a conclusion that the weakly turbulent chimera is a macroscopic spatiotemporal chaotic state. It is non-extensive in dependence on the parameter N : the largest Lyapunov exponent and the number of positive exponents (as well as other quantities like Kaplan-Yorke dimension) remain finite in the limit $N \rightarrow \infty$.

6. Conclusion

Summarizing, we have studied a one-dimensional medium of identical phase oscillators with asymmetric in space nonlocal coupling. The considered setup generalizes the Abrams–Strogatz chimera model. We have found exact traveling wave solutions moving at constant velocities with permanent shapes in the continuous limit and studied their stability. Such regular nontrivial traveling wave solutions appear as unevenly (nonuniformly) twisted synchronized states. Only in specific ranges of parameters some of these waves are linearly stable. For the corresponding parameters, such traveling wave patterns appear as attractors in finite populations despite the finite-size deviations from the continuous limit. In other parameter domains, no stable traveling waves exist and although such a wave can be temporarily observed, in particular, during initial evolution starting from the standing chimera, it is destroyed and a weakly turbulent traveling chimera is established due to instability. We have checked that this turbulence is not a finite-size effect (like chaos in a standing chimera) by calculating the Lyapunov spectrum and showing that the largest Lyapunov exponent of the system remains size-independent, starting from a certain number of units. The weak turbulent chimera exists for long time intervals. Still, in some regions of parameters, we observed a transition to a fully synchronous state or to a regular (uniformly or nonuniformly) twisted wave. We have shown that the traveling wave solutions play an essential role in the emerging process of the turbulent regime because of their time-intermittent appearance. Using direct numerical simulations, we have also shown that the traveling chaotic chimera states are at least transient with a very long lifetime.

Data availability statement

The data that support the findings of this study are available upon reasonable request from the authors. The data cannot be made publicly available upon publication because they are not available in a format that is sufficiently accessible or reusable by other researchers.

Acknowledgments

The authors thank O Omel'chenko and K Krischer for fruitful discussions. L A S and M I B were supported by the Russian Science Foundation (sections 2 and 3, Project No. 22-12-00348) and the Ministry of Science and Higher Education of the Russian Federation (sections 4 and 5, Project No. 0729-2020-0036).

ORCID iDs

L A Smirnov  <https://orcid.org/0000-0002-2293-6534>

M I Bolotov  <https://orcid.org/0000-0001-9561-2357>

A Pikovsky  <https://orcid.org/0000-0001-9682-7122>

References

- [1] Panaggio M J and Abrams D M 2015 *Nonlinearity* **28** R67
- [2] Omel'chenko O E 2013 *Nonlinearity* **26** 2469
- [3] Omel'chenko O E 2018 *Nonlinearity* **31** R121
- [4] Kuramoto Y and Battogtokh D 2002 *Nonlinear Phenom. Complex Syst.* **5** 380
- [5] Abrams D M and Strogatz S H 2004 *Phys. Rev. Lett.* **93** 174102
- [6] Ott E and Antonsen T M 2008 *Chaos* **18** 037113
- [7] Laing C R 2009 *Physica D* **238** 1569
- [8] Bordyugov G, Pikovsky A and Rosenblum M 2010 *Phys. Rev. E* **82** 035205
- [9] Smirnov L, Osipov G and Pikovsky A 2017 *J. Phys. A: Math. Theor.* **50** 08LT01

- [10] Bolotov M I, Smirnov L A, Osipov G V and Pikovsky A 2020 *Phys. Rev. E* **102** 042218
- [11] Bolotov D I, Bolotov M I, Smirnov L A, Osipov G V and Pikovsky A S 2022 *Radiophys. Quantum Electron.* **64** 709
- [12] Smirnov L A, Bolotov M I, Bolotov D I, Osipov G V and Pikovsky A 2022 *New J. Phys.* **24** 043042
- [13] Omel'chenko O E 2019 *J. Phys. A: Math. Theor.* **52** 104001
- [14] Omel'chenko O E 2022 *Nonlinearity* **36** 845
- [15] Wiley D A, Strogatz S H and Girvan M 2006 *Chaos* **16** 015103
- [16] Girnyk T, Hasler M and Maistrenko Y 2012 *Chaos* **22** 013114
- [17] Omel'chenko O E, Wolfrum M and Laing C R 2014 *Chaos* **24** 023102
- [18] Xie J, Knobloch E and Kao H-C 2014 *Phys. Rev. E* **90** 022919
- [19] Bolotov D, Bolotov M, Smirnov L, Osipov G and Pikovsky A 2019 *Regul. Chaotic Dyn.* **24** 717
- [20] Lee S and Krischer K 2022 *Phys. Rev. E* **106** 044210
- [21] Smirnov L A, Osipov G V and Pikovsky A 2018 *Phys. Rev. E* **98** 062222
- [22] Dudkowski D, Czołczyński K and Kapitaniak T 2019 *Nonlinear Dyn.* **95** 1859
- [23] Bick C and Martens E A 2015 *New J. Phys.* **17** 033030
- [24] Smirnov L and Pikovsky A 2023 *Phil. Trans. R. Soc. A* **381** 20220076
- [25] Omel'chenko O E 2019b *Nonlinearity* **33** 611
- [26] Campos J 1997 *Bull. London Math. Soc.* **29** 205
- [27] Wilczyński P 2008 *J. Differ. Equ.* **244** 1304
- [28] Marvel S A, Mirollo R E and Strogatz S H 2009 *Chaos* **19** 043104
- [29] Gong C C, Toenjes R and Pikovsky A 2020 *Phys. Rev. E* **102** 022206
- [30] Omel'chenko O E 2022 *J. Nonlinear Sci.* **32** 22
- [31] Dziubak V, Maistrenko Y and Schöll E 2013 *Phys. Rev. E* **87** 032907
- [32] Omel'chenko O E and Knobloch E 2019 *New J. Phys.* **21** 093034
- [33] Pikovsky A and Politi A 2016 *Lyapunov Exponents. A Tool to Explore Complex Dynamics* (Cambridge University Press)
- [34] Omel'chenko O E, Wolfrum M and Maistrenko Y L 2010 *Phys. Rev. E* **81** 065201
- [35] Wolfrum M, Omel'chenko O E, Yanchuk S and Maistrenko Y L 2011 *Chaos* **21** 013112
- [36] Wolfrum M and Omel'chenko O E 2011 *Phys. Rev. E* **84** 015201